

Calculation of Resonance Energy Transfer in Crowded Biological Membranes

Daniel B. Zimet,* Bernard J.-M. Thevenin,* A. S. Verkman,[‡] Stephen B. Shohet,* and James R. Abney*[§]

*Department of Laboratory Medicine and [‡]Cardiovascular Research Institute, University of California, San Francisco, California 94143; and

[§]Department of Physics, Lewis and Clark College, Portland, Oregon 97219 USA

ABSTRACT Analytical and numerical models were developed to describe fluorescence resonance energy transfer (RET) in crowded biological membranes. It was assumed that fluorescent donors were linked to membrane proteins and that acceptors were linked to membrane lipids. No restrictions were placed on the location of the donor within the protein or the partitioning of acceptors between the two leaflets of the bilayer; however, acceptors were excluded from the area occupied by proteins. Analytical equations were derived that give the average quantum yield of a donor at low protein concentrations. Monte Carlo simulations were used to generate protein and lipid distributions that were linked numerically with RET equations to determine the average quantum yield and the distribution of donor fluorescence lifetimes at high protein concentrations, up to 50% area fraction. The Monte Carlo results show such crowding always reduces the quantum yield, probably because crowding increases acceptor concentrations near donor-bearing proteins; the magnitude of the reduction increases monotonically with protein concentration. The Monte Carlo results also show that the distribution of fluorescence lifetimes can differ markedly, even for systems possessing the same average lifetime. The dependence of energy transfer on acceptor concentration, protein radius, donor position within the protein, and the fraction of acceptors in each leaflet was also examined. The model and results are directly applicable to the analysis of RET data obtained from biological membranes; their application should result in a more complete and accurate determination of the structures of membrane components.

INTRODUCTION

Fluorescence resonance energy transfer (RET) is widely used as a “spectroscopic ruler” to determine submicroscopic (10–100 Å) associations and distances in biological samples (Stryer, 1978; Fairclough and Cantor, 1978; Eftink, 1991). For example, RET has been used to monitor binding reactions, protein folding, and phase transitions, as well as to map intra- and intermolecular distances between labeled sites in macromolecular assemblies (Stryer, 1978; Eftink, 1991). Distance measurement using RET exploits the fact that the transfer of excited-state energy from a single fluorescent donor to a single acceptor depends on the inverse sixth power of the separation between donor and acceptor. Therefore, donor/acceptor separation can be deduced from the efficiency of energy transfer.

Unfortunately, in some biological samples, energy transfer occurs simultaneously between donor/acceptor pairs having different separations, greatly complicating data interpretation. For example, in studies of biological membranes, the donor is typically a fluorescently labeled protein that is capable of transferring energy to many lipophilic acceptors, each at a different distance from the protein. In this case, a model must be used to quantify the relationship between the observed energy transfer efficiency and the distribution of donor/acceptor distances. Analytical approximations for

RET efficiencies in membranes have been derived using models that assume that the lipophilic probes distribute uniformly in the plane of the membrane and that the donor is attached to a single protein at a point located in the plane of the membrane (Wolber and Hudson, 1979) or at some fixed distance above the membrane (Shaklai et al., 1977; Kleinfeld, 1985; Yguerabide, 1994). Analytical solutions for other configurations, which are intended to model energy transfer between lipid bilayers and between vesicles, have also been derived (Koppel et al., 1979; Dewey and Hammes, 1980).

In biological membranes, a significant fraction of membrane area (~20–50%) is typically occupied by proteins (Saxton, 1989), and the assumption of uniform lipid distribution implicit in the above models is violated. Descriptions of RET in biological membranes must quantify these non-uniformities and incorporate them into a more realistic model. Unfortunately, these generalized models are not amenable to purely analytical solutions; instead, numerical techniques such as Monte Carlo simulations must be used to describe the nonuniformities in lipid and protein distribution and then the numerical data used to calculate energy transfer efficiencies. Several studies have examined the special case in which acceptors are excluded from protein aggregates containing donors (Gutierrez-Merino, 1981; Dewey and Data, 1989; Kubitschek et al., 1993); however, treatment of the aggregates requires specific geometrical modeling and the acceptors are assumed to be distributed uniformly away from the aggregates. Snyder and Freire (1982) attempted a more general solution involving nonuniform donors and acceptors, but their approach was later shown (Jan et al., 1984) to be valid only under very restrictive (nonequilibrium) conditions not representative of membranes.

Received for publication 6 September 1994 and in final form 12 January 1995.

Address reprint requests to James R. Abney, Department of Physics, Lewis & Clark College, Portland, OR 97219. Tel.: 503-768-7585; Fax: 503-768-7369; E-mail: bethe@lclark.edu.

© 1995 by the Biophysical Society

0006-3495/95/04/1592/12 \$2.00

In this work, we have used Monte Carlo techniques to simulate a fluid membrane in which donor fluorophores are linked at arbitrary positions to membrane proteins and in which acceptor fluorophores are linked to lipids in one or both leaflets of the membrane bilayer. Monte Carlo simulations were used to generate the equilibrated coordinates of the donors and acceptors; estimates of RET quenching ratios and lifetime distributions were calculated directly from these coordinates. These results are compared with those obtained from an analytical model capable of describing energy transfer from an arbitrarily located donor to uniformly distributed acceptors at low protein concentrations.

THEORY

Fluorescence RET refers to the transfer of excited-state energy from a fluorescent donor to an acceptor. Energy transfer provides a route for depopulating the excited state of the donor and so reduces both the donor quantum yield and donor fluorescence lifetime. Theories of energy transfer relate the reduction in quantum yield and lifetime to interesting physical properties of the system, including intra- and intermolecular distances.

Equations for donor quantum yield and lifetime

In an RET experiment, a donor molecule is excited from its ground state into its first excited state by the absorption of a photon. The excited-state energy can be lost through a variety of mechanisms, including production of a photon (fluorescence), quenching, intersystem crossing, and energy transfer (Lakowicz, 1983). The rate of decay of the excited state, $P(t)$, through these mechanisms can be described by a simple first-order differential equation

$$\frac{dP(t)}{dt} = -(\Gamma + k + k_{ET})P(t) \quad (1)$$

where Γ describes the rate of intrinsic (radiative) decay, k describes the rate of competing (nonradiative) processes including intersystem crossing and quenching, and k_{ET} describes the rate of energy transfer. The functional form for k_{ET} was derived by Förster (1948) for weak dipole-dipole coupling between donor and acceptor, and is given by

$$k_{ET} = \tau_D^{-1} \sum_{i=1}^{N_A} \left(\frac{R_0}{r_i} \right)^6 \quad (2)$$

Here $\tau_D = 1/(\Gamma + k)$ is the donor lifetime in the absence of acceptors, N_A is the number of acceptors, r_i is the separation between the donor and acceptor i , and R_0 is the Förster distance, the separation at which 50% of excited state decay proceeds through energy transfer (i.e., the separation at which $k_{ET} = 1/\tau_D$). The solution of Eq. 1 is

$$P(t) = \exp[-(\Gamma + k + k_{ET})t] \quad (3)$$

$$= \exp\left(-\frac{t}{\tau_D}\right) \prod_{i=1}^{N_A} \exp\left[-\left(\frac{t}{\tau_D}\right)\left(\frac{R_0}{r_i}\right)^6\right]$$

Both the donor quantum yield and donor fluorescence lifetime can be derived from Eq. 3. It is customary to focus on the change in donor properties induced by energy transfer; thus, relative quantum yields and fluorescence lifetimes are determined as ratios of values in the presence and absence of energy transfer. The relative quantum yield for a single donor, q_r , is given by

$$q_r = \frac{q_{DA}}{q_D} = \frac{\int_0^\infty P_{DA}(t) dt / \int_0^\infty P_0(t) dt}{\int_0^\infty P_D(t) dt / \int_0^\infty P_0(t) dt} \quad (4)$$

$$= \frac{\Gamma + k}{\Gamma + k + k_{ET}} = \left[1 + \sum_{i=1}^{N_A} \left(\frac{R_0}{r_i} \right)^6 \right]^{-1}$$

where $P_{DA}(t)$ describes donor decay in the presence of acceptors, $P_D(t)$ in the absence of acceptors, and $P_0(t)$ in the absence of nonradiative pathways (i.e., when $k = k_{ET} = 0$). If N_D donors are present, the average quantum yield, Q_r , can be determined by averaging Eq. 4 over each donor to give

$$Q_r = \frac{1}{N_D} \sum_{j=1}^{N_D} q_{r,j} = \frac{1}{N_D} \sum_{j=1}^{N_D} \left[1 + \sum_{i=1}^{N_A} \left(\frac{R_0}{r_{ij}} \right)^6 \right]^{-1} \quad (5)$$

The relative donor lifetime can be found in similar fashion, yielding

$$\tau_r = \frac{1}{N_D} \sum_{j=1}^{N_D} \frac{\tau_{DA,j}}{\tau_{D,j}} = \frac{1}{N_D} \sum_{j=1}^{N_D} \frac{[\int_0^\infty t P_{DA}(t) dt / \int_0^\infty P_{DA}(t) dt]_j}{[\int_0^\infty t P_D(t) dt / \int_0^\infty P_D(t) dt]_j} \quad (6)$$

$$= \frac{1}{N_D} \sum_{j=1}^{N_D} \left[1 + \sum_{i=1}^{N_A} \left(\frac{R_0}{r_{ij}} \right)^6 \right]^{-1}$$

Note that the relative quantum yield equals the relative donor lifetime, $Q_r = \tau_r$.

Eqs. 5 and 6 for the donor quantum yield and fluorescence lifetime are exact, assuming several mild conditions are met. First, the number of fluorophores in the excited state at any given time must be small compared to the total number of fluorophores. In this case, there will be no competition between donors for transfer to a given acceptor, and all acceptors will be continuously available for transfer. This is generally the case in fluorescence measurements. Second, energy transfer must occur nonradiatively and without reversible transfer from acceptors to donors. Third, the number of proteins labeled with donor must be sufficiently small that donor-donor transfer can be neglected. Finally, the value of R_0 must be identical and unchanging for each donor/acceptor pair, corresponding to energy transfer in either the static or dynamic limit. (This constraint can be relaxed in our numerical model, if an appropriate model of donor and acceptor orientation is available.)

Ensemble averages

RET experiments generally involve the measurement of Q_r or τ_r as a function of acceptor concentration. To deduce donor-to-acceptor distances from RET measurements, a model is used to predict donor and acceptor positions and then to evaluate Eqs. 5 and 6; the validity of the model is

assessed by comparing theoretical and experimental results. In membrane systems, donor and acceptor positions fluctuate; Eqs. 5 and 6 must then be ensemble averaged over the statistical distributions of donors and acceptors.

Ensemble averaging can be performed two ways using statistical mechanics: analytically, or numerically by Monte Carlo simulation. If the averaging is performed in the canonical ensemble, the probability of each possible configuration of donors and acceptors can be assumed to be proportional to the Boltzmann factor, $\exp[-U(\{\vec{r}\})/k_B T]$. Here k_B is Boltzmann's constant, T is the temperature, and $U(\{\vec{r}\})$ is an energy function that describes the interactions among membrane components located at positions \vec{r}_1 through \vec{r}_N . Analytical values of $\langle Q_r \rangle$ or $\langle \tau_r \rangle$ are found by integrating the variable of interest, weighted by the Boltzmann factor, over all possible configurations; here $\langle \rangle$ denotes an ensemble average. For example,

$$\langle Q_r \rangle = \frac{\int \cdots \int Q_r(\{\vec{r}\}) \exp[-U(\{\vec{r}\})/k_B T] d\vec{r}_1 \cdots d\vec{r}_N}{\int \cdots \int \exp[-U(\{\vec{r}\})/k_B T] d\vec{r}_1 \cdots d\vec{r}_N} \quad (7)$$

Eq. 7 can seldom be simplified. Instead, numerical estimates of $\langle Q_r \rangle$ must be found using Monte Carlo simulations (Hansen and McDonald, 1986). In this approach, an "importance sampling" algorithm is used to generate configurations with probabilities given by the Boltzmann factor. Ensemble-averaged values of Q_r are then determined by computing Q_r for each configuration so generated, and then directly averaging the result without further weighting. Energetically favored ("important") configurations appear most often and so contribute most heavily to the average. Details of the Monte Carlo algorithm are given under Methods.

Analytical expressions for single-donor energy transfer

For a single volume-excluding fluorescent donor and randomly distributed noninteracting acceptors, it is possible to derive an analytical expression for $\langle Q_r \rangle$. The derivation of this equation is given in the Appendix; the associated model is shown in Fig. 1. The donor (*) is fixed to a cylindrical protein of radius R_p at a height H and a distance ϵR_p from the protein axis, where ϵ is referred to as the eccentricity. Acceptors are attached to lipids represented as points confined to one or two planes (leaflets) normal to the protein axis. For a single layer of acceptors, the limiting case $H = 0$ corresponds to the donor lying within the plane of the acceptors, while the case $R_p = 0$ corresponds to the acceptors not being restricted from any region of the membrane.

The relative quantum yield for the single-donor case is given by

$$Q_r = \int_0^\infty \exp \left\{ -\lambda + \sum_{l=1}^2 \sigma_l \left[\pi \beta_l - \int_0^\pi \left[\alpha_l^{1/3} e^{-\lambda/\alpha_l} + \lambda^{1/3} \gamma \left(\frac{2}{3}, \frac{\lambda}{\alpha_l} \right) \right] d\theta \right] \right\} d\lambda \quad (8a)$$

where σ_l is the acceptor concentration (in units of acceptor

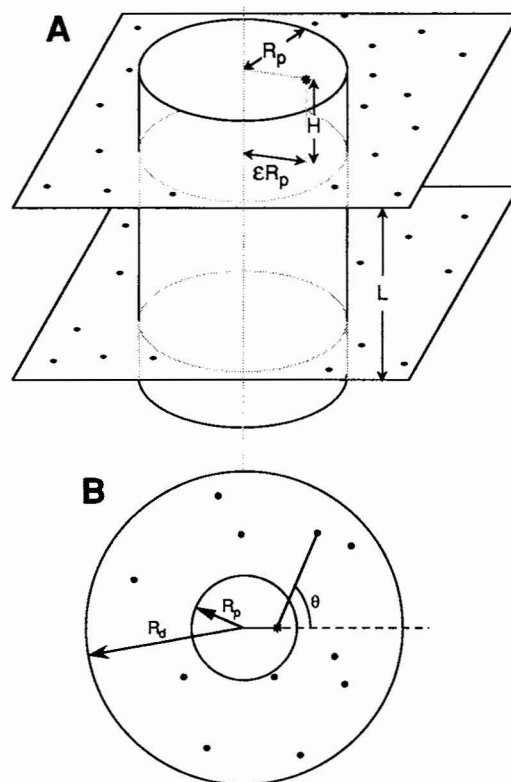


FIGURE 1 Model and coordinate system used in energy transfer calculations. (A) Perspective view. The donor (*) is attached to a cylindrical protein whose principal axis is assumed to be normal to the plane of the bilayer. The acceptors (•) are distributed within one or both leaflets of the bilayer. (B) Top view. Donor/acceptor separations were characterized by a distance, r , and a polar angle, θ . In the single-donor (absence of crowding) case, acceptors were confined to an annulus bounded by R_p and R_d . In the multiple-donor (presence of crowding) case, acceptors and donors were confined to a square cell.

number/ R_0^2) in leaflet l , $\gamma(a, x)$ is the incomplete gamma function defined by the variable-limit integral

$$\gamma(a, x) = \int_0^x t^{a-1} e^{-t} dt \quad (8b)$$

and α and β are combinations of geometrical parameters

$$\alpha_l = \{H_l^2 + R_p^2 [\epsilon \cos \theta - (1 - \epsilon^2 \sin^2 \theta)^{1/2}]\}^3 / R_0^6 \quad (8c)$$

$$\beta_l = (H_l^2 + R_p^2) / R_0^2 \quad (8d)$$

with $H_l = H$ for one leaflet and $H + L$ for the other. The derivation of Eq. 8 is given in the Appendix.

Simpler versions of Eq. 8 describe energy transfer in systems in which only one leaflet contains acceptors or in which the eccentricity in donor position is 0. If both of these conditions are met, Eq. 8 can be rewritten as a single integral

$$\langle Q_r \rangle = \int_0^\infty \exp \left\{ -\lambda - \pi \sigma \left[\gamma \left(\frac{2}{3}, \frac{\lambda}{\alpha} \right) \lambda^{1/3} - \alpha^{1/3} (1 - e^{-\lambda/\alpha}) \right] \right\} d\lambda \quad (9a)$$

where

$$\alpha = (H^2 + R_p^2)^3 / R_0^6 \quad (9b)$$

If $H = 0$, Eq. 9 is identical to an expression originally derived by Wolber and Hudson (1979) to describe energy transfer between coplanar donor and acceptors. Eq. 9 must still be evaluated numerically, although exponential fits (Wolber and Hudson, 1979) and continued-fraction approximants (Dewey and Hammes, 1980) have been derived to describe certain limiting cases.

METHODS

Energy transfer in the absence of protein crowding

Single-donor energy transfer in the absence of crowding was studied both analytically and numerically. Analytical expressions, Eqs. 8 and 9, were evaluated using Mathematica (Wolfram Research Inc., Champaign, IL). Numerical simulations were performed by choosing acceptor positions at random within an annulus bounded by R_p and R_a ; see Fig. 1. The inner cutoff represents the protein diameter, whereas the outer cutoff represents the physical extent of the membrane, which was always taken to be $>6R_0$. The relative quantum yield, $\langle Q_r \rangle$, was then computed from acceptor and donor coordinates using Eq. 4. This process was repeated and the results averaged using Eq. 5 until the standard deviation in $\langle Q_r \rangle$ was $<1\%$.

Energy transfer in the presence of protein crowding

Energy transfer in the presence of crowding was studied using a Monte Carlo approach. This procedure yields "snapshots" of donor and acceptor positions, from which the relative quantum yield and distribution of donor lifetimes can be determined by direct evaluation of Eqs. 4–6.

Protein coordinates were generated using the standard Metropolis et al. (1953) Monte Carlo algorithm. Simulations were performed on 256 proteins in a square cell; the size of the cell determined the protein concentration. Edge effects were avoided by using permeable cell boundaries and periodic boundary conditions (Hansen and McDonald, 1986). "Equilibrated" protein configurations were generated by randomly perturbing protein positions and accepting new positions that did not lead to overlap with other proteins. This approach yields protein coordinates indistinguishable from those in a physical system in which proteins interact through excluded-volume interactions. The proteins were initially equilibrated for 50,000 Monte Carlo cycles; a cycle corresponds to one sequentially attempted move of each protein. After the equilibration steps, a series of 500 coordinate sets was generated, each separated from the last by 100 cycles. This process was repeated for each protein concentration used.

Energy transfer calculations for a given protein concentration were performed on randomly chosen subsets of these 500 coordinate sets. First, a coordinate set was chosen, and donor positions within the proteins were assigned at a fixed distance eR_p from the protein center and at random angles between 0 and 2π . Next, acceptor coordinates were chosen randomly, as in the single-donor case. The acceptors were treated as points, but were restricted from overlapping with the donor disks. Acceptors were confined to a single plane or divided between two planes, corresponding to a bilayer labeled on one or both leaflets, respectively. Finally, from the generated coordinates, the relative quantum yield, q_r , of each donor in the ensemble was calculated using Eq. 4. The summation in Eq. 4 was performed over all acceptors within the cell; the side length of the cell was always $>6R_0$. Since $q_{r,j} = \tau_{r,j}$ the distribution of fluorescence lifetimes in the system could be determined by constructing a histogram of q_r values. The values of q_r were averaged using Eq. 5 to obtain $\langle Q_r \rangle$. This process was repeated for enough protein configurations to bring the standard deviation in $\langle Q_r \rangle$ below 1%; this required 6,400–25,600 estimates. This procedure was repeated for each choice of R_p , σ , H , and ϵ .

Radial distribution functions

The statistical distribution of proteins and acceptors in the presence of crowding was summarized using the radial distribution function, $g(r)$. Radial distribution functions were computed by averaging the interparticle separations in the coordinate sets over discrete bins; details of the algorithm are described elsewhere (Abney and Scalettar, 1993). Distribution functions served two purposes. First, they were compared with limiting-case analytical expressions to test the Monte Carlo algorithm. Second, they provide insight into donor and acceptor distribution that is necessary to interpret the RET results.

RESULTS

In this section, we examine the dependence of $\langle Q_r \rangle$ and τ_r on 1) acceptor concentration, 2) protein concentration, 3) protein radius, 4) donor position within the protein, and 5) one-versus two-leaflet labeling. For convenience, R_p and H are normalized by the Förster distance, R_0 , and σ is normalized by R_0^2 . Acceptor concentrations are reported per total membrane area, not total lipid area; thus, for a given acceptor concentration, there are the same number of acceptors in each system, independent of protein concentration.

Energy transfer in the absence of protein crowding

Single-donor energy transfer in the absence of crowding was calculated analytically, using Eqs. 8 and 9, and numerically, using Monte Carlo simulations. In this case, lipids are only excluded from that portion of the membrane occupied by the single protein bearing the donor.

Centrally located donor

If the donor is located at the center of the protein (i.e., $\epsilon = 0$), then the relative quantum yield, $\langle Q_r \rangle$, will depend only on the acceptor concentration, σ , and the distance of closest approach between donor and acceptors, $R_e \equiv (R_p^2 + H^2)^{1/2}$. Fig. 2 shows that the quantum yield decreases monotonically as the acceptor concentration increases and as the distance between donor and acceptors decreases. Results derived from the analytical and Monte Carlo approaches are in agreement.

These exact results were compared with two analytical approximations describing single-donor energy transfer; see Fig. 2. These approximations are commonly used in place of Eq. 9 because they do not require numerical integration. The first approximation is a two-exponential fit to Eq. 9 (Eq. 17 and Table I; Wolber and Hudson, 1979). This expression is valid for $\sigma < 0.5$ and $R_e < 1.3 R_0$, but it significantly overestimates the transfer efficiency outside this range. The second approximation is a third-order analytical approximant to Eq. 9, originally derived for point-to-plane transfer (Eqs. 22–24; Dewey and Hammes, 1980). This expression is valid for $R_e > 1.0$; outside this range the expression overestimates the transfer efficiency for small σ and significantly underestimates the transfer efficiency for larger σ . Note that, although neither analytical expression is valid for all σ and R_p , the two

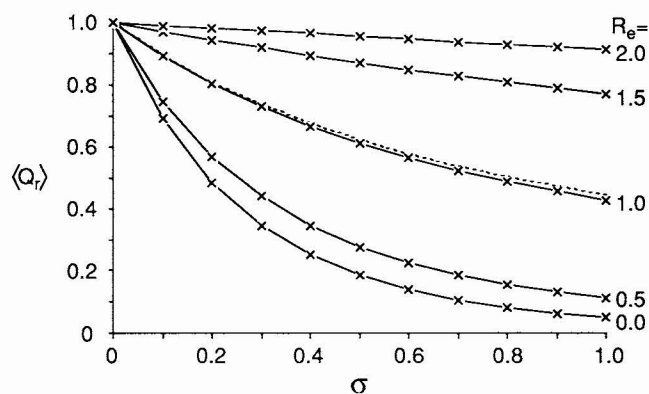


FIGURE 2 Relative quantum yield for energy transfer from a single centrally located donor as a function of acceptor concentration. Values obtained from the analytical expression, Eq. 9, are denoted by \times . Values obtained from numerical simulations, using only a single donor and 256 acceptors, are connected by solid lines; numerical values were obtained every $\sigma = 0.1$. Note that transfer efficiency depends on $R_e \equiv (R_p^2 + H^2)^{1/2}$; $\langle Q_r \rangle$ will be the same for any combination of R_p and H that gives the same value of R_e . For comparison, results derived in two previous studies are also plotted. Values obtained from a third-order analytical approximant (Dewey and Hammes, 1980) for $R_p = 1.0, 1.5$, and 2.0 are connected by dashed lines. Values obtained from a two-exponential fit to Eq. 9 (Wolber and Hudson, 1979) for $R_p = 0.0, 0.5$, and 1.0 are connected by dotted lines. Note that many of the approximate results are hidden beneath the solid line due to their close agreement with the numerical results. The third-order approximant underestimates energy transfer for small R_e , whereas the two-exponential fit overestimates energy transfer for large R_e . The error in the third-order approximant is $\sim 160\%$ for $R_e = 0.5$ and $\sigma = 1$; the error in the two-exponential fit is $\sim 10\%$ for $R_e = 1.3$ and $\sigma = 1$.

expressions are complementary and can be combined to give a reasonable description of energy transfer over the range of conditions plotted in Fig. 2.

Eccentrically located donor

In most experimental situations, the donor is not located precisely at the center of the protein (i.e., $\epsilon \neq 0$). The relative quantum yield then depends on σ , R_p , H , and ϵ ; it is no longer possible to subsume the dependence on R_p and H into the single variable R_e . Fig. 3 A shows that the quantum yield decreases as the donor gets closer to the edge of the protein (i.e., as ϵ increases). Results derived from the analytical and Monte Carlo approaches are in good agreement, although there is a small ($<7\%$) disparity when R_p and ϵ are both large.

Two-leaflet labeling

In some experimental situations, acceptors may be deliberately or inadvertently introduced into both leaflets of the bilayer. Acceptors may be deliberately introduced to provide data from a different geometric configuration that can complement single-leaflet data. Alternatively, acceptors may be inadvertently introduced due to acceptor flip-flop or if both sides of the membrane are accessible during labeling. The description of two-leaflet labeling requires consideration

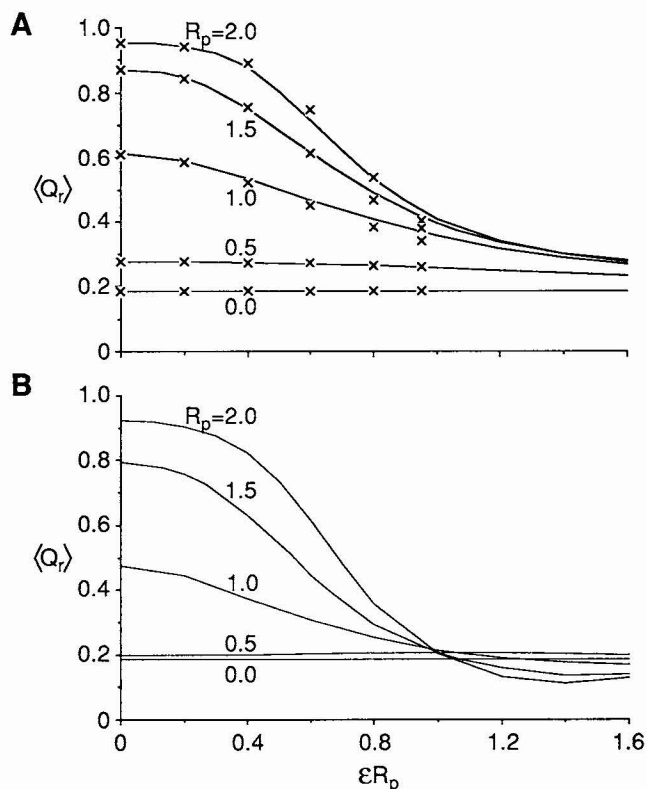


FIGURE 3 Relative quantum yield for energy transfer from an eccentrically located donor as a function of eccentricity in donor location. (A) Quantum yields for 0% area fraction. Values obtained from the analytical expression, Eq. 8 ($l = 1$), are denoted by \times . Values obtained from numerical simulations are connected by the solid lines. (B) Quantum yields for 50% area fraction. Results were obtained by Monte Carlo simulation. In both panels, $H = 0$ and $\sigma = 0.5$. Under some experimental situations, a donor may extend beyond the radius of a cylindrical protein; an example would be a donor attached to a narrow tether. To describe such situations, values of $\langle Q_r \rangle$ corresponding to $\epsilon > 1$ have been included in the plot. However, because it was assumed during the Monte Carlo simulations that proteins were cylindrical, excluded-volume interactions among portions of proteins that extend beyond R_p when $\epsilon > 1$ were implicitly neglected.

of two new variables: the fraction of the total acceptor concentration in each leaflet, and the leaflet-leaflet separation. The leaflet-leaflet separation is determined by the portion of the lipid to which the label is attached. Fig. 4 shows quantum yield as a function of leaflet separation. When the leaflet-leaflet separation is zero, the quantum yield is equal to that for a single leaflet with the combined acceptor concentration. When the leaflet-leaflet separation is very large, the quantum yield is determined only by energy transfer to the closer leaflet. Because energy transfer falls off as the inverse sixth power of the donor/acceptor separation, energy transfer at intermediate separations is dominated by the closer leaflet. Note that calculation of the quantum yield requires simultaneous consideration of both leaflets; it is not possible to obtain the two-leaflet result simply by combining quantum yields for two independent leaflets at different separations, as is evident by an examination of Eq. 8. Two-leaflet results

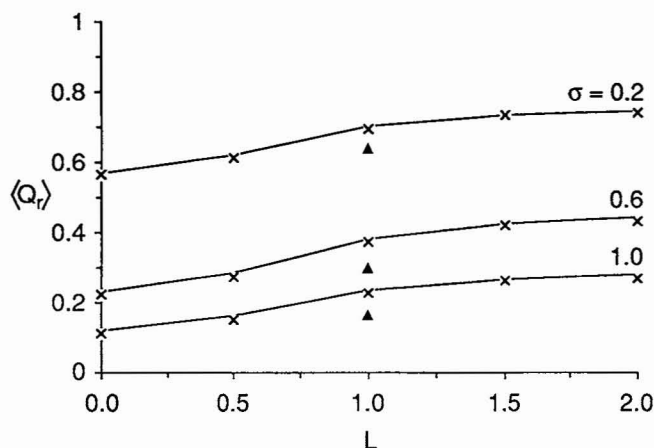


FIGURE 4 Relative quantum yield for energy transfer to acceptors in two leaflets as a function of leaflet separation. Results are shown for $R_p = 0.5$, $H = 0$, and $\sigma = 0.2, 0.6$, and 1.0 as indicated; acceptors are partitioned equally between the two leaflets. Values obtained from the analytical expression, Eq. 8 ($l = 2$), are denoted by \times . Values obtained from numerical simulations (under identical conditions) are connected by the solid lines. These analytical and numerical results describe single-donor transfer in the absence of protein crowding. Also shown (\blacktriangle) are results describing energy transfer in the presence of crowding ($A_f = 50\%$) for $L = 1.0$ and σ as indicated; quantum yields for area fractions between 0 and 50% lie between these two values.

derived here from both analytical and numerical approaches are in agreement.

Radial distribution functions

The single-donor model neglects a universal characteristic of biological membranes: the high concentration of membrane proteins. Crowding at high protein concentrations influences the organization of membrane proteins and lipids, which in turn influences the extent of energy transfer. In this section, the effects of crowding on protein and acceptor distribution are briefly reviewed.

If the membrane behaves like a simple fluid, then the relative positions of membrane proteins and lipids can be statistically summarized using distribution functions (Abney and Scalettar, 1993). The relative positions of pairs of molecules within the membrane are described by the radial distribution function, $g(r)$. The radial distribution function gives a measure of the probability of finding a second particle at a distance r from a given first particle. Fig. 5 A shows $g(r)$ for hard-disk proteins in the coordinate sets used in subsequent calculations of quantum yield and lifetime. The distribution functions show that relative protein positions are sensitive functions of protein concentration. As protein concentration is increased, coordination shells build around each protein, and the average interprotein spacing decreases. This latter effect can be attributed to an effective protein-protein force. The highest values of $g(r)$ are obtained at protein-protein separations corresponding to contact; these values agree to within 2% with previously published contact values

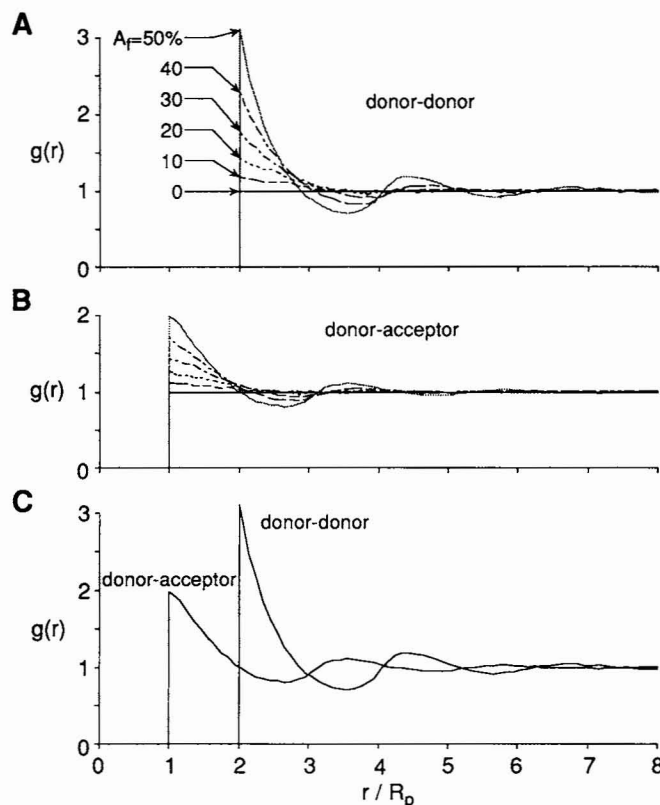


FIGURE 5 Radial distribution functions of donors and acceptors. (A) Monte Carlo generated distributions of donors. Data were averaged over discrete bins of width $0.1 R_p$. The radial distribution function measures the probability of finding a particle at a distance r from a given particle. At small separations, less than the excluded-volume diameter, the probability of finding a second particle is 0 ($g(r) = 0$). At large separations, the probability of finding a second particle is random ($g(r) = 1$), as there are no long-range correlations in fluids. At intermediate separations, there are coordination shells corresponding to regions of enhanced ($g(r) > 1$) and diminished ($g(r) < 1$) probabilities of finding a second particle. The radial distribution function depends on the interparticle force, the temperature, and the particle concentration. At low particle concentrations, correlations in particle positions are weak and $g(r) \approx 1$ for all separations. However, at high particle concentrations, such as those typical of biological membranes, correlations in particle positions are strong and $g(r)$ can display several coordination shells. (B) Monte Carlo generated distributions of acceptors. The distribution functions reflect the probability of finding an acceptor at a distance r from a given donor. Binning was identical to that used in (A). (C) Correlations between donor and acceptor distributions. This figure compares the radial distribution functions for donors and acceptors at 50% area fraction protein. Note that acceptor and donor positions are negatively correlated.

based on analytical theory (Abney et al., 1989), confirming that the Monte Carlo algorithm was implemented correctly.

Fig. 5 B shows $g(r)$ for the acceptors relative to a protein in the same coordinate sets. These curves indicate that acceptor positions are also sensitive to protein concentration and that acceptors are arrayed in coordination shells around the proteins. Fig. 5 C shows that lipid and protein positions are anticorrelated: annuli with high protein concentrations have low lipid concentrations, and vice versa. At small separations corresponding to contact, both lipid and protein concentrations are enhanced. However, since the peaks in the

two distribution functions fall at different separations, lipid and protein concentrations are not simultaneously enhanced.

Energy transfer in the presence of protein crowding

The single-donor case can be contrasted with energy transfer between donors and acceptors whose distribution is perturbed by excluded-volume interactions; see Fig. 6.

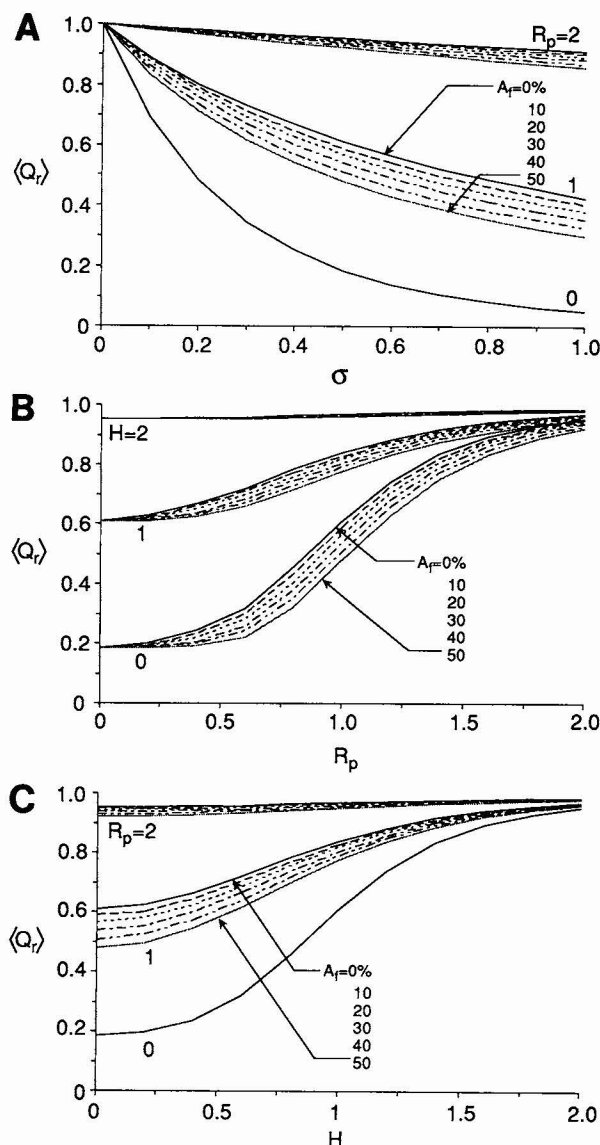


FIGURE 6 Relative quantum yield for energy transfer from a centrally located donor in the presence of excluded-volume protein-protein interactions. (A) Relative quantum yield as a function of acceptor concentration. Values were obtained every $\sigma = 0.1$ for $H = 0$ and R_p and A_f as indicated. (B) Relative quantum yield as a function of protein radius. Values were obtained every $R_p = 0.2$ for $\sigma = 0.5$ and H and A_f as indicated. (C) Relative quantum yield as a function of donor height above the membrane. Values were obtained every $H = 0.2$ for $\sigma = 0.5$ and R_p and A_f as indicated. Under all conditions displayed here, crowding acts to decrease quantum yield. Note also that crowding breaks the symmetry between H and R_p that is manifest at 0% area fraction.

Centrally located donor

When crowding is important, energy transfer is no longer a simple function of the distance of closest approach between donor and acceptor; instead, donor height and radius must be considered separately. This distinction becomes necessary because crowding introduces correlations in acceptor positions that scale with protein radius but not with donor height.

Consider first donor-in-plane transfer ($H = 0$). Fig. 6 A shows that the quantum yield decreases with increasing acceptor concentration and decreasing protein radius, as in the single-donor case. In addition, the quantum yield also decreases with increasing protein concentration. The magnitude of this decrease depends on protein radius, as shown in Fig. 6 B. The absolute difference in quantum yield between systems at 0% and 50% area fraction, defined as $[\langle Q_r \rangle(0\%) - \langle Q_r \rangle(50\%)]$, starts at 0 for $R_p = 0$, rises to a maximum for $R_p \sim R_0$, and then decays toward 0 as $R_p \rightarrow \infty$. In contrast, the relative difference in quantum yield, defined as $[\langle Q_r \rangle(0\%) - \langle Q_r \rangle(50\%)]/[1 - \langle Q_r \rangle(0\%)]$, increases monotonically over the range of radii examined, with no evidence of a maximum. Hence, crowding contributes a more significant fraction of the change in $\langle Q_r \rangle$ at larger protein radii.

The dependence of quantum yield on protein crowding and protein size can be understood in terms of acceptor distribution (see Fig. 5). Since nearby acceptors contribute most heavily to the decrease in quantum yield, crowding always enhances energy transfer because it always enhances the number of acceptors near the donor. The degree of enhancement depends on protein size because correlations in protein and acceptor positions are dictated by R_p and not by R_0 , and because contributions to $\langle Q_r \rangle$ fall off very quickly with increasing r . For small proteins, there is little change in $\langle Q_r \rangle$ because the small coordination shells contain relatively few acceptors, even when enhanced by crowding. Furthermore, energy is transferred to acceptors in several coordination shells and intervening troughs, so that the integrated contribution is similar to that from a uniform distribution. For large proteins, there is little absolute change in $\langle Q_r \rangle$ because there is little energy transfer at large distances. However, there is a significant relative change because essentially only the first annulus contributes to $\langle Q_r \rangle$, and the number of acceptors in this large annulus is considerably enhanced by crowding. Finally, when the protein is of intermediate size ($R_p \approx R_0$), the first shell is large enough to contain significant numbers of acceptors and close enough to contribute significantly to the quantum yield, leading to a maximum in the absolute enhancement in energy transfer.

Consider next donor-off-plane transfer ($H > 0$). Fig. 6 C shows that the quantum yield decreases with decreasing donor height and increasing area fraction. Qualitatively, the dependence on donor height is similar to the dependence on protein radius discussed above, with one significant difference. The absolute difference in quantum yield between systems at 0% and 50% area fraction displayed a maximum for increasing R_p . In contrast, this difference decreases monotonically for increasing H . The disparity arises because an

increase in H simply increases the distance between donor and acceptor, reducing energy transfer, whereas an increase in R_p changes the scaling of the correlations in acceptor distribution, bringing into play the competing factors discussed above. For this same reason, in the presence of crowding, $\langle Q_r \rangle$ is no longer a function only of $R_e \equiv (R_p^2 + H^2)^{1/2}$, as it is in the absence of crowding. Instead, $\langle Q_r \rangle$ depends on the precise combination of R_p and H . For example, for $R_e = 2$, $\langle Q_r \rangle(H=2, R_p=0) > \langle Q_r \rangle(H=\sqrt{2}, R_p=\sqrt{2}) > \langle Q_r \rangle(H=0, R_p=2)$.

Eccentrically located donor

Next consider the general case of energy transfer from an eccentrically placed donor ($\epsilon \neq 0$). Fig. 3 *B* shows that quantum yield decreases with increasing donor eccentricity and decreasing protein radius, again in qualitative agreement with the single-donor case. A comparison of Fig. 3, *A* and *B* shows that the quantum yield also decreases with increasing protein concentration. This occurs because higher protein concentrations lead to higher acceptor concentrations near the edge of the protein, enhancing energy transfer and reducing quantum yield. Again, the magnitude of this enhancement depends on protein size and reflects the differences in scaling between size and distribution. Most interestingly, for proteins of intermediate size ($R_p \approx R_0$), energy transfer can be enhanced over energy transfer from both larger and smaller proteins, as manifest in the crossover in the energy curves for $\epsilon \approx 1$ in Fig. 3 *B*. The crossover reflects an interplay between positional correlations that scale with R_p and transfer efficiencies that scale with R_0 , as was described for the central donor.

Two-leaflet labeling

The qualitative features of energy transfer to two leaflets of acceptors are not significantly altered by crowding; see Fig. 4. Most transfer again occurs to acceptors in the closer leaflet. The primary difference in the presence of crowding is that changes in L , like changes in H , do not lead to a rescaling in acceptor distribution, while changes in R_p do.

Lifetime distributions

Because the average quantum yield in the presence of energy transfer depends on many variables including donor geometry and donor/acceptor distribution, it is possible for different experimental conditions to give rise to the same average quantum yield. This has important experimental consequences, because a single measurement of average quantum yield may not distinguish between the different combinations of variables that can lead to the same $\langle Q_r \rangle$. In principle, this difficulty could be overcome by experimentally perturbing some variable, such as acceptor concentration, and then using a model to predict what overall set of conditions would give rise to any observed changes. An alternative approach might involve measurement of the fluo-

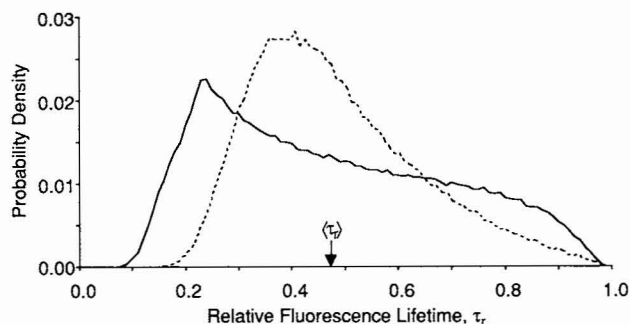


FIGURE 7 Distribution of relative fluorescence lifetimes. Plot shows the distribution of relative fluorescence lifetimes associated with two energy transfer scenarios possessing the same average lifetime, 0.47, as indicated by the arrow. Data are divided into bins of width 0.01 and correspond to $\epsilon = 0$, $\sigma = 0.5$, and either (—) $A_f = 0.1$, $R_p = 0.2$, and $H = 0.8$ or (---) $A_f = 0.5$, $R_p = 1.0$, and $H = 0$. Histograms are normalized such that the total integrated probability equals unity.

rescence lifetime, in addition to the quantum yield. Unfortunately, measurement of the average lifetime will not provide additional information, because the average lifetime is equal to the average quantum yield (see Eqs. 5 and 6). However, an analysis of the distribution of fluorescence lifetimes, instead of just the average lifetime, may distinguish between different scenarios possessing the same average lifetime.

Fig. 7 shows the distribution of lifetimes for two systems differing significantly in protein concentration ($A_f = 0.1$ vs. 0.5), protein size ($R_p = 0.2$ vs. 1.0), and donor height ($H = 0.8$ vs. 0). Both systems possess the same average lifetime, but nonetheless display significantly different lifetime distributions. These distributions can be computed from the simulation data used in the computation of average quantum yields. The average lifetimes (or average quantum yields) presented in Figs. 2–4 and 6 were determined by computing the lifetime of each donor for each donor/acceptor configuration, and then averaging the results. If instead of averaging these lifetimes are sorted into bins, a distribution of lifetimes can be determined. Note that whenever there is a distribution of donor/acceptor separations, there will be a distribution of fluorescence lifetimes, even in the absence of crowding. Unfortunately, measurement of very complicated lifetime distributions is probably not feasible using current technology.

Energy transfer in the presence of soft-repulsive and long-range attractive interactions

Because the protein-protein interactions dictating protein distribution in an experimental system are seldom known, it is important to determine how energy transfer is influenced by the nature of the interaction potential. Here, energy transfer in the presence of excluded-volume interactions will be compared with energy transfer in the presence of long-range attractions and repulsions. Purely repulsive and attractive-plus-repulsive potentials were generated by a WCA decom-

position (Chandler et al., 1983) of an inverse-power-law potential (Abney et al., 1989).

$$u(r) = \frac{27}{4} k_B T \left[\left(\frac{\sigma}{r} \right)^6 - \left(\frac{\sigma}{r} \right)^4 \right] \quad (10)$$

Here σ (not to be confused with the acceptor concentration) defines the zero crossing of the potential, and $k_B T$ gives the depth of the attractive well in the attractive potential. These two potentials approximate the weak, long-range attractions and soft repulsions predicted to act between proteins in bilayer membranes (Abney and Scalettar, 1993). Monte Carlo simulations were run on 256 particles to generate protein distributions at low ($\rho^* = \rho\sigma^2 = 0.3$) and high ($\rho^* = 0.8$) reduced densities; acceptor distributions and the quantum yield were then computed as described for the excluded-volume interactions. Acceptors were excluded from regions within σ of the protein centers.

The quantum yield at a given reduced density was nearly identical for the two long-range potentials (data not shown), despite the fact that the associated protein distributions differ significantly at low density (Abney and Scalettar, 1993). This suggests that the primary effect of crowding on energy transfer is to enrich the acceptor population near the proteins, thereby decreasing quantum yield. This enrichment is observed for all potentials, so crowding always decreases quantum yield.

DISCUSSION

The goal of this study was to develop a description of RET between a donor site on a membrane protein and bilayer-distributed acceptors for experimentally important donor-acceptor geometries and biologically realistic protein concentrations. Previous studies have focused on energy transfer from a single, centrally located donor to randomly distributed lipid acceptors. From a practical viewpoint, the generality of these expressions is limited because donor fluorophores are often attached to proteins at noncentral locations and because acceptor positions can be significantly perturbed by the high concentrations of membrane proteins. These two shortcomings were addressed in the current study. First, general analytical expressions were derived describing energy transfer from a donor arbitrarily located on a membrane protein to randomly distributed acceptors in the absence of other proteins. Second, Monte Carlo simulations were employed to characterize the effects of crowding-induced changes in acceptor organization on energy transfer. The results of the current study can be used directly in the interpretation of experimental data, or to estimate the error in quantities derived using the previous theories.

The influence of protein crowding on energy transfer was simulated by populating part of the membrane with proteins, and restricting acceptor coordinates to the remaining (lipid-phase) regions of the membrane. Energy transfer is therefore a function not only of acceptor concentration and protein size, as in the single-donor case, but also of protein distribution. In biological membranes, protein distribution de-

pends on many parameters, including protein concentration, protein-protein interactions, and extramembranous attachments. However, if the membrane is assumed to behave like a simple two-dimensional fluid, then equilibrium protein positions can be simulated knowing only protein concentration and the protein-protein interaction by using the standard Metropolis et al. (1953) Monte Carlo algorithm. The coordinates generated by Monte Carlo simulation are indistinguishable from those that would be observed in an equilibrated system at the specified concentration and interacting through the chosen potential.

The analytical results presented in this paper are essentially exact within the confines of energy transfer theory. However, the numerical results are subject to a few minor caveats. Most serious among these is that, because the true protein-protein, protein-lipid, and lipid-lipid interactions are not known, the simulations had to be run using model potentials. However, most of the results were generated using excluded-volume interactions, which are known to reproduce the most important effects of interactions on protein organization (Abney and Scalettar, 1993) and diffusion (Scalettar and Abney, 1991). In addition, the energy transfer results obtained for two very different inverse-power-law potentials were very similar to one another and to the results obtained using the excluded-volume interaction; this suggests that crowding effects on RET are dominated by protein concentration, and not the precise interaction potential. For this reason, the Monte Carlo results may also give a reasonable description of membranes in which some fraction of the proteins are immobile.

The distribution of fluorescence lifetimes was shown to be capable of distinguishing between different sets of RET parameters yielding the same average lifetime. Accurate modeling of lifetime distributions hinges on two assumptions. First, the random fluctuations in acceptor positions must be taken into account; this is because a different lifetime is associated with each configuration. All of the numerical simulations in this paper properly treat acceptor fluctuations. In contrast, because the analytical results were derived by assuming that the distribution of acceptors was continuous, they can only yield an average fluorescence lifetime. Second, the distribution of donors and acceptors should be approximately constant during the lifetime of the excited state; this is equivalent to stating that the donors and acceptors should not diffuse very far over a time scale equal to the fluorescence lifetime. The root-mean-square displacement of a molecule, r_{rms} , undergoing two-dimensional Brownian diffusion is given by the expression $r_{\text{rms}} = (4Dt)^{1/2}$, where D is the diffusion coefficient and t is the time (Scalettar and Abney, 1991). Typical fluorescence lifetimes will be shorter than ~ 4 ns. Similarly, typical diffusion coefficients for acceptors attached to lipids in biological membranes will be $\sim 10^{-8}$ cm²/s; diffusion coefficients for donors attached to membrane proteins may be much smaller (McCloskey and Poo, 1986). These values predict that donors and acceptors will typically move ~ 1 Å or less while the fluorophore remains

in an excited state. Such small-scale motions should not preclude comparison with lifetime distributions predicted from static donor/acceptor configurations.

Computational limitations necessitated performing the Monte Carlo simulation in two steps, with proteins equilibrated first as interacting particles and lipids equilibrated second as noninteracting (ideal) particles. This two-step procedure requires justification, since ideally one would equilibrate both components simultaneously to account for all interparticle interactions. This procedure can be justified by noting that the protein-protein interaction used in the simulation of protein positions can be assumed to represent an "effective" interaction that formally includes the effects of protein-lipid and lipid-lipid interactions (Abney and Scalettar, 1993). For this reason, the protein positions accurately reflect the presence of the lipids. Moreover, the positions of labeled lipids can be assigned randomly without introducing error because the total area fraction of labeled lipids is so small ($\leq 2\%$). A two-step equilibration process can also be justified on dynamic grounds. Membrane proteins typically diffuse much more slowly than membrane lipids. Consequently, lipid molecules probably quickly re-equilibrate in response to any changes in protein distribution.

A number of checks were performed to confirm the validity of the simulation results. First, it was shown that the particle distributions (measured by $g(r)$) used in the calculations were identical to those for distributions equilibrated for 10 times more and 1/10 as many steps, ensuring that the particles were properly equilibrated before data were collected. Second, the cell in which simulations were run always extended farther than the correlations displayed in the distribution functions, ensuring that particles could not interact with themselves through the periodic boundaries. Finally, there were always at least 256 proteins and 256 lipids, ensuring that fluctuations arising from small numbers of particles were minimal.

The model presented here permits quantification of the effects of protein and lipid distribution on energy transfer between a protein-bound donor and the lipid bilayer. The amount of energy transfer is affected by lipid exclusion from various regions of the membrane. The most significant effect on energy transfer is due to lipid exclusion by the protein bearing the donor; this always reduces energy transfer because acceptors are pushed away from the donor. In contrast, lipid exclusion by other proteins in the membrane invariably increases energy transfer because acceptors are pushed toward the protein bearing the donor. Neglecting excluded area will thus introduce significant error into energy transfer measurements; the error is especially severe if the donor is attached to a large protein, as was the case in RET studies of the chloroplast coupling factor, the IgE-F ϵ R1 receptor complex, and the nicotinic acetylcholine receptor (summarized in Mitra and Hammes, 1990; Zheng et al., 1991; Johnson et al., 1990). Although RET has been used to characterize the structure of over a dozen membrane components, only work on the (Ca²⁺-Mg²⁺)-ATPase (for a summary see Stefanova

et al., 1993; Corbalan-Garcia et al., 1993), cytochrome b₅ (Fleming et al., 1979; Kleinfeld and Lukacovic, 1985), and recently on the nicotinic acetylcholine receptor (Valenzuela et al., 1994) has attempted to account for lipid exclusion by the protein bearing the donor. These studies were, however, all subject to the approximations inherent in purely analytical approaches.

RET distance measurements between specific protein sites and the bilayer have contributed greatly to our understanding of the geometry, orientation, and conformation of membrane components. However, an accurate determination of intermolecular distances in membrane systems requires consideration of the nonuniform distribution of acceptor lipids resulting from protein-lipid and protein-protein interactions. The analytical expression for energy transfer derived here (Eq. 8) accounts for interactions between acceptors and the protein bearing the donor. This equation is a good and convenient approximation at low protein concentrations, even if two leaflets of the bilayer are labeled and the position of the donor on the membrane protein is noncentral; this expression becomes virtually exact if the component under study is reconstituted at low protein-lipid ratios. However, in studies of real biological membranes, in which the area fraction of protein usually exceeds 20% (Saxton, 1989), a numerical model of energy transfer is needed to describe accurately the effects of interactions among all components of the membrane.

APPENDIX

Analytical solution for energy transfer from an eccentrically located donor

An analytical expression for the relative quantum yield of a single eccentrically located donor in the presence of one or two planes of randomly located acceptors can be derived from Eqs. 3, 4, and 7. The approach taken here parallels that used by Wolber and Hudson (1979) for the special case described by Eq. 9 and complements that recently adopted by Yguerabide (1994). Consider first energy transfer to a single plane of acceptors; in this case, the ensemble-averaged quantum yield is given by

$$\langle Q_i \rangle = \frac{1}{\tau_D} \int_0^\infty \langle P_{DA}(t) \rangle dt \quad (\text{A1a})$$

where

$$\langle P_{DA}(t) \rangle = \frac{\mathcal{A}}{\int \cdots \int \exp[-U(\{\vec{r}\})/k_B T] d\vec{r}_1 \cdots d\vec{r}_N} \quad (\text{A1b})$$

where

$$\mathcal{A} = \int \cdots \int \exp\left(-\frac{t}{\tau_D} \prod_{i=1}^{N_A} \exp\left[-\left(\frac{t}{\tau_D}\right) \left(\frac{R_0}{r_i}\right)^6\right]\right) \exp\left[-\frac{U(\{\vec{r}\})}{k_B T}\right] d\vec{r}_1 \cdots d\vec{r}_N$$

Fortunately, Eq. A1b can be simplified considerably. For a

hard-disk protein, the lipid-protein interaction $U(\{\vec{r}\})$ is zero over allowed donor/acceptor separations; the exponentials involving $U(\{\vec{r}\})$ thus equal unity for these separations. Furthermore, for a single plane of acceptors, the integrations over all N donor/acceptor pairs are independent and identical. Consequently, Eq. A1b can be rewritten as

$$\langle P(t) \rangle = \exp(-t/\tau)[J(t)]^N \quad (\text{A2a})$$

where $J(t)$ is defined as

$$J(t) = \frac{\int \exp[-(t/\tau)(R_0/r)^6] d\vec{r}}{\int d\vec{r}} \quad (\text{A2b})$$

The remainder of the derivation consists primarily of simplifying Eq. A2b.

The integrals in Eq. A2b can only be partially evaluated. The integral in the denominator is simply the area occupied by acceptors, which equals the area of the annulus bounded by R_p and R_d , $\pi(R_d^2 - R_p^2)$. To evaluate the integral in the numerator, it is convenient to introduce a polar angle θ as defined in Fig. 1 B; this facilitates the determination of the angle-dependent limits of integration on the donor/acceptor separation, r . For each θ , the minimum and maximum values of r , which are determined by H , R_p , and R_d , can be calculated using the Law of Cosines. The integral in the numerator can then be written

$$J(t) = \frac{\int_0^{2\pi} I(\theta) d\theta}{\pi(R_d^2 - R_p^2)} \quad (\text{A3a})$$

where

$$I(\theta) = \int_{r_{\min}(\theta)}^{r_{\max}(\theta)} \exp\left[-\left(\frac{t}{\tau}\right)\left(\frac{R_0}{r}\right)^6\right] r dr \quad (\text{A3b})$$

$$r_{\min, \max}(\theta) = \{H^2 + R_{p,d}^2[\epsilon \cos \theta - (1 - \epsilon^2 \sin^2 \theta)^{1/2}]\}^{1/2} \quad (\text{A3c})$$

$I(\theta)$ can be rewritten by introducing the change of variables $\chi = (t/\tau)(R_0/r)^6$ and integrating by parts. The result is

$$I(\theta) = -\frac{1}{2}\left(\frac{t}{\tau}\right)^{1/3} R_0^2 \left[\chi_p^{-1/3} \exp(-\chi_p) - \chi_d^{-1/3} \exp(-\chi_d) - \gamma\left(\frac{2}{3}, \chi_d\right) + \gamma\left(\frac{2}{3}, \chi_p\right) \right] \quad (\text{A4})$$

where $\gamma(2/3, \chi_{p,d})$ is the variable-limit gamma function defined by Eq. 8b, and χ_p and χ_d correspond to χ evaluated at r_{\min} and r_{\max} , respectively. The arbitrary limit, R_d , on acceptor positions can be relaxed by taking the limit $R_d \rightarrow \infty$, which yields

$$I(\theta) = -\frac{1}{2}\left(\frac{t}{\tau}\right)^{1/3} R_0^2 \left[\chi_p^{-1/3} \exp(-\chi_p) - \chi_d^{-1/3} + \gamma\left(\frac{2}{3}, \chi_p\right) \right] \quad (\text{A5})$$

Substituting Eq. A5 back into Eq. A3a and evaluating

integrals analytically whenever possible yields

$$J(t) = 1 + \frac{1}{N} \left\{ \frac{\sigma}{2} \left[2\pi(H^2 + R_p^2) - R_0^2 \int_0^\pi \left[\alpha^{1/3} e^{-\lambda/\alpha} + \lambda^{1/3} \gamma\left(\frac{2}{3}, \frac{\lambda}{\alpha}\right) \right] d\theta \right] \right\} \quad (\text{A6a})$$

where α is given by Eq. 8c and

$$\lambda = t/\tau \quad (\text{A6b})$$

$$\sigma = N[\pi(R_d^2 - R_p^2)] \quad (\text{A6c})$$

The expression for $J(t)$ can now be substituted back into Eq. A2a to determine $\langle P(t) \rangle$. In the limit that $R_d \rightarrow \infty$, the number of acceptors N also becomes large. Making use of the expression

$$\lim_{N \rightarrow \infty} \left(1 + \frac{a}{N} \right)^N = e^a \quad (\text{A7})$$

gives

$$Q_t = \exp(\pi\sigma\beta) \int_0^\infty \exp\left\{ -\lambda - \sigma \times \int_0^\pi \left[\alpha^{1/3} e^{-\lambda/\alpha} + \lambda^{1/3} \gamma\left(\frac{2}{3}, \frac{\lambda}{\alpha}\right) \right] d\theta \right\} d\lambda \quad (\text{A8})$$

where β is given by Eq. 8d.

Eq. A8 describes the quantum yield for energy transfer from an eccentric donor to a single plane of randomly distributed acceptors; the generalization to describe energy transfer to two planes of acceptors is straightforward. Eq. A2 becomes a product of two different integrals, one for each leaflet. Each integral is raised to a power given by the number of acceptors in the associated leaflet, and both integrals are identical except for the limits of integration, which reflect the difference in bilayer separation ($H \rightarrow H + L$ in Eq. A3c for the leaflet farther from the donor). The integrals are evaluated as described above for the single-leaflet case. The final result is a product of exponentials, which can be rewritten as an exponential of a sum, yielding Eq. 8 in the text.

We gratefully acknowledge helpful conversations with Drs. Daniel Axelrod, Stephen Bicknese, James Corbett, Thomas Olsen, John Owicki, Michael Saxton, and Bethe Scalettar. We would also like to thank Bethe Scalettar for a critical reading of the manuscript and Lewis and Clark College for the use of its computational facilities.

This work was supported by grants DK16095 and DK43840 from the National Institutes of Health and a grant-in-aid from the MacMillan Trust. J. R. Abney was partially supported by training grant HL07185. This is publication 133 from the MacMillan-Cargill Hematology Research Laboratory.

REFERENCES

- Abney, J. R., and B. A. Scalettar. 1993. Molecular crowding and protein organization in biological membranes. In *Thermodynamics of Membrane Receptors and Channels*. M. B. Jackson, editor. CRC Press, Boca Raton, Florida. 183-226.

- Abney, J. R., B. A. Scalettar, and J. C. Owicki. 1989. Mutual diffusion of interacting membrane proteins. *Biophys. J.* 56:315–326.
- Chandler, D., J. D. Weeks, and H. C. Andersen. 1983. Van der Waals picture of liquids, solids, and phase transformations. *Science*. 220: 787–794.
- Corbalan-Garcia, S., J. A. Teruel, and J. C. Gomez-Fernandez. 1993. Intramolecular distances within the Ca^{2+} -ATPase from sarcoplasmic reticulum as estimated through fluorescence energy transfer between probes. *Eur. J. Biochem.* 217:737–744.
- Dewey, T. G., and M. M. Data. 1989. Determination of the fractal dimension of membrane protein aggregates using fluorescence energy transfer. *Biophys. J.* 56:415–420.
- Dewey, T. G., and G. G. Hammes. 1980. Calculation of fluorescence resonance energy transfer on surfaces. *Biophys. J.* 32:1023–1036.
- Eftink, M. R. 1991. Fluorescence techniques for studying protein structure. In *Methods of Biochemical Analysis: Protein Structure Determination*, Vol. 35. H. C. Suelter, editor. John Wiley and Sons, New York. 127–204.
- Fairclough, R. H., and C. R. Cantor. 1978. The use of singlet-singlet energy transfer to study macromolecular assemblies. *Methods Enzymol.* 48:347–379.
- Fleming, P. J., D. E. Koppel, A. L. Y. Lau, and P. Strittmatter. 1979. Intramembrane position of the fluorescent tryptophanyl residue in membrane-bound cytochrome b_5 . *Biochemistry*. 18:5458–5464.
- Förster, T. 1948. Zwischenmolekulare Energiewanderung und Fluoreszenz. *Ann. Physik.* 2:55–75.
- Gutierrez-Merino, C. 1981. Quantitation of the Förster energy transfer for two-dimensional systems. II. Protein distribution and aggregation state in biological membranes. *Biophys. Chem.* 14:259–266.
- Hansen, J. P., and I. R. McDonald. 1986. Computer “experiments” on liquids. In: *Theory of Simple Liquids*, 2nd ed. Academic Press, London, 45–68.
- Jan, N., T. Lookman, and D. A. Pink. 1984. On computer simulation methods used to study models of two-component lipid bilayers. *Biophys. J.* 23:3227–3231.
- Johnson, D. A., R. Cushman, and R. Malekzadeh. 1990. Orientation of cobra α -toxin on the nicotinic acetylcholine receptor: fluorescence studies. *J. Biol. Chem.* 265:7360–7368.
- Kleinfeld, A. M. 1985. Tryptophan imaging of membrane proteins. *Biochemistry*. 24:1874–1882.
- Kleinfeld, A. M., and M. F. Lukacovic. 1985. Energy-transfer study of cytochrome b_5 using the anthroxlyoxy fatty acid membrane probes. *Biochemistry*. 24:1883–1890.
- Koppel, D. E., P. J. Fleming, and P. Strittmatter. 1979. Intramembrane positions of membrane-bound chromophores determined by excitation energy transfer. *Biochemistry*. 18:5450–5457.
- Kubitscheck, U., R. Schweitzer-Stenner, D. J. Arndt, T. M. Jovin, and I. Pecht. 1993. Distribution of type I Fc_ϵ -receptors on the surface of mast cells probed by fluorescence resonance energy transfer. *Biophys. J.* 64:110–120.
- Lakowicz, J. R. 1983. *Principles of Fluorescence Spectroscopy*. Plenum Publishing Co., New York.
- McCloskey, M. A., and M.-m. Poo. 1986. Rates of membrane-associated reactions: reduction of dimensionality revisited. *J. Cell Biol.* 102:88–96.
- Metropolis, N., A. W. Rosenbluth, M. N. Rosenbluth, A. H. Teller, and E. Teller. 1953. Equations of state calculations by fast computing machines. *J. Chem. Phys.* 21:1087–1092.
- Mitra, B., and G. G. Hammes. 1990. Membrane-protein structural mapping of chloroplast coupling factor in asolectin vesicles. *Biochemistry*. 29: 9879–9884.
- Saxton, M. J. 1989. Lateral diffusion in an archipelago: distance dependence of the diffusion coefficient. *Biophys. J.* 56:615–622.
- Scalettar, B. A., and J. R. Abney. 1991. Molecular crowding and protein diffusion in biological membranes. *Comm. Mol. Cell. Biophys.* 7:79–107.
- Shaklai, N., J. Yguerabide, and H. M. Ranney. 1977. Interaction of hemoglobin with red blood cell membranes as shown by a fluorescent chromophore. *Biochemistry*. 16:5585–5592.
- Snyder, B., and E. Freire. 1982. Fluorescence energy transfer in two dimensions: a numeric solution for random and nonrandom distributions. *Biophys. J.* 40:137–148.
- Stefanova, H. I., A. M. Mata, M. G. Gore, J. M. East, and A. G. Lee. 1993. *Biochemistry*. 32:6095–6103.
- Stryer, L. 1978. Fluorescence energy transfer as a spectroscopic ruler. *Annu. Rev. Biochem.* 47:819–846.
- Valenzuela, C. F., P. Weign, J. Yguerabide, and D. A. Johnson. 1994. Transverse distance between the membrane and the agonist binding sites on the *Torpedo* acetylcholine receptor: a fluorescence study. *Biophys. J.* 66: 674–682.
- Wolber, P. K., and B. S. Hudson. 1979. An analytic solution to the Förster energy transfer problem in two dimensions. *Biophys. J.* 28:197–210.
- Yguerabide, J. 1994. Theory for establishing proximity relations in biological membranes by excitation energy transfer measurements. *Biophys. J.* 66:683–693.
- Zheng, Y., B. Shopes, D. Holowka, and B. Baird. 1991. Conformations of IgE bound to its receptor $\text{Fc}\epsilon\text{RI}$ and in solution. *Biochemistry*. 30:9125–9132.